PAPER

Cite this: *RSC Adv.*, 2021, **11**, 15351

Performance of gamma-Al$_2$O$_3$ decorated with potassium salts in the removal of CS$_2$ from C$_5$ cracked distillate

Xiance Zhang, [ID] [a] Guanglin Zhou,*[a] Mengying Wang,[b] Xiaosheng Wang, [ID] [a] Weili Jiang[a] and Hongjun Zhou[a]

Deep desulfurization is a key process for the production of high value-added products from C$_5$ distillates. In this work, different potassium salt modified gamma-Al$_2$O$_3$ adsorbents were prepared by an incipient-wetness impregnation method and characterized by N$_2$ adsorption–desorption, SEM-EDS, TEM, CO$_2$-TPD, XRD, FT-IR, and IC. The C$_5$ distillate with a 1200 μg mL^{-1} sulfur content is desulfurized to less than 10 μg mL^{-1} within 24 hours by the static adsorption method. For the desulfurization in the fix-bed reactor, the breakthrough sulfur capacity of K$_2$CO$_3$-decorated gamma-Al$_2$O$_3$ reaches 0.76 wt% under the optimized conditions, *viz.*, at 30 °C, with a sulfur content of 50 μg mL^{-1} in the raw oil, and a liquid hourly space velocity of 1 h^{-1}. The desulfurization activity of the exhausted adsorbent can be recovered after regeneration. Selective adsorption of CS$_2$ includes three processes: adsorption, hydrolysis, and oxidation. CS$_2$ is first adsorbed on the adsorbent and hydrolyzed to form H$_2$S. H$_2$S is further oxidized to form S/SO$_4^{2-}$, and then deposits on the surface of the adsorbent. Adsorption, hydrolysis, and oxidation all play essential roles in the removal process of CS$_2$.

1 Introduction

C$_5$ distillate is one of the by-products of high-temperature cracking of naphtha to ethylene.[1] Its yield is generally about 14–20% that of ethylene. C$_5$ contains nearly 20 kinds of compounds, including isoprene, cyclopentadiene, and piperylene.[2] Their unique molecular structures can be used to synthesize other chemical products, which have high economic value.[3] In the petrochemical industry, two technologies are commonly used to treat the C$_5$: one method is to separate it into monomers; another way is to use it as a raw material for producing low-carbon olefins after hydrogenation.

The sulfur composition of C$_5$ is different compared with other distillates. When naphtha is cracked to ethylene, it is easy to coke due to the high temperature during the pyrolysis process, which affects the product quality. Salari *et al.*[4] found that different types of sulfides have different effects on coking performance. At a certain sulfur content, the coking rate is as follows: dimethyl disulfide (DMDS) < disulfide oil < dimethyl sulfide < CS$_2$. To reduce the amount of coke and prolong the cracking furnace operating cycle, DMDS and CS$_2$ are selected as coking inhibitors to reduce the coking rate in the industrial production process. Therefore, the main sulfide in the C$_5$ is CS$_2$, with a small number of other sulfides

such as thioether, mercaptan, and thiophene. The existence of sulfur compounds greatly impacts the physical properties of catalysts, additives, and products, as well as the processing stability and the value of the products. Although the sulfur content of C$_5$ varies (often in the range of 40–100 μg mL^{-1}) from different manufacturers, the main sulfide is always CS$_2$.

In traditional desulfurization technology, the more mature hydrodesulfurization technology results in unnecessary olefin saturation, excessive sulfur species,[5] which is not suitable for the C$_5$. Compared with traditional hydrogen desulfurization, adsorption desulfurization has the advantages of a short process, low energy consumption, and no hydrogen required.[6–8] However, the C$_5$ adsorption desulfurization has not achieved large-scale industrialization due to the insufficient experimental data and unclear desulfurization mechanism. Patent CN101450303A[9] reported a method of adsorbents preparation, they mixed group 8 and group 11 metal salts with sodium hydroxide as the precipitant in an aprotic solvent, then mixed with the Al$_2$O$_3$ dry glue to obtain the adsorbent. Under certain conditions, the adsorbent could remove almost all sulfide in C$_5$ conjugated diene raw materials. However, this desulfurization process requires hydrogen and a higher operating temperature, which leads to the saturation and polymerization of C$_5$ olefin. Patent CN103182291A[10] used the pseudo-boehmite powder to prepare gamma-Al$_2$O$_3$ support and then impregnated a mixed solution of Zn^{2+}, Cu^{2+}, group 1, or group 2 metal to obtain a desulfurization adsorbent. The desulfurization of the cracked C$_5$ using a fixed bed can reduce the sulfur content to 1 μg g^{-1} or lower. However, the adsorbent sulfur capacity is low, and regeneration is difficult.

[a]College of New Energy and Materials, China University of Petroleum-Beijing, Beijing, 102249, China. E-mail: zhouguanglin2@163.com
[b]College of Chemical Engineering and Environment, China University of Petroleum-Beijing, Beijing, 102249, China

The methane reaction with sulfur and hydrogen sulfide is considered the leading cause of undesirable CS_2 in the modified Claus process.[11] A highly efficient hydrolysis catalyst is required to remove CS_2 and COS. The reactions of CS_2 hydrolysis are as follows:[12] $CS_2 + H_2O \rightarrow COS + H_2S$, $COS + H_2O \rightarrow CO_2 + H_2S$, $CS_2 + 2H_2O \rightarrow CO_2 + 2H_2S$. The C_5 contains a trace amount of water, and the hydrolysis reaction of CS_2 may occur. Therefore, using a hydrolysis catalyst to remove CS_2 from the C_5 would be an effective method.[13,14] In this paper, the gamma-Al_2O_3 support is loaded with different potassium salts by an incipient-wetness impregnation method. The C_5 distillate is used as raw material. Static adsorption experiments and fixed bed dynamic experiments are carried out to study the adsorption performance of the modified adsorbent on CS_2. Furthermore, the desulfurization mechanism is investigated by N_2 adsorption–desorption, SEM-EDS, TEM, XRD, CO_2-TPD, FT-IR, and IC.

2 Results and discussion

2.1 Performance of catalysts in static experiments

Fig. 1 shows the desulfurization performance of gamma-Al_2O_3 adsorbents decorated by three different potassium salt solutions. The Al_2O_3 can remove the CS_2 in C_5, and the sulfur content in C_5 is 989 $\mu g\ mL^{-1}$ after 3 hours. After the calcination at 500 °C, the KNO_3 in the KNO_3/Al_2O_3 catalyst decomposes into K_2O and form an Al–O–K structure with Al_2O_3.[15] However, the adsorption desulfurization ability of KNO_3/Al_2O_3 is slightly improved, only 16 $\mu g\ mL^{-1}$ higher after 3 hours. The KOH/Al_2O_3 and K_2CO_3/Al_2O_3 improve the adsorption and desulfurization ability of the Al_2O_3 support significantly, indicating that the alkaline has good selective adsorption for CS_2. The modified Al_2O_3 is more alkaline than Al_2O_3, which corresponds to the subsequent CO_2-TPD characterization. The desulfurization effect of K_2CO_3/Al_2O_3 is better than that of KOH/Al_2O_3. When the adsorption time is 3 hours, the sulfur content in the product is 412 $\mu g\ mL^{-1}$ and 496 $\mu g\ mL^{-1}$, respectively. The cause of this phenomenon is analyzed in the next section.

Fig. 2 shows the effect of adsorbents prepared by different concentrations of K_2CO_3 on the removal performance of CS_2.
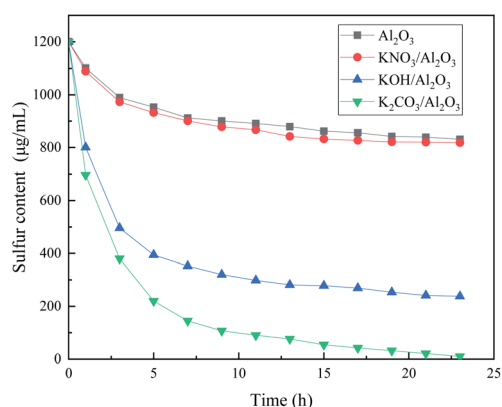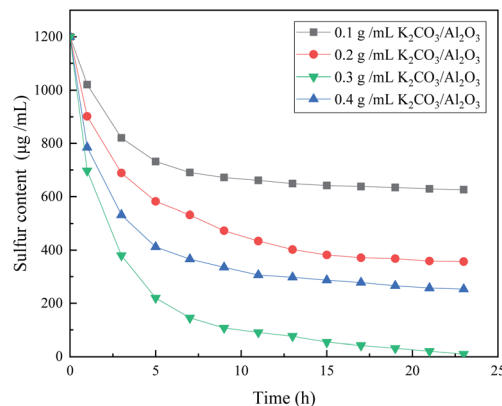
Fig. 2 Removal performance of CS_2 over Al_2O_3 modified by different K_2CO_3 concentration.

The desulfurization capacity gradually increases with the increase of K_2CO_3 impregnation concentration. When the impregnation concentration of K_2CO_3 is 0.3 $g\ mL^{-1}$, the static desulfurization performance is the greatest, and the sulfur content in C_5 can be reduced to less than 10 $\mu g\ mL^{-1}$ from 1200 $\mu g\ mL$; however, continue increasing the impregnation concentration K_2CO_3 results in decreasing of the desulfurization capacity. This indicates that the amount of alkali has a significant influence on the desulfurization activity. The loading of K_2CO_3 affects the alkalinity of the adsorbent surface and the distribution of basic sites in the desulfurizer. The weak base center on the surface of adsorbent is more critical, and the strong alkalinity is not conducive to the adsorption of CS_2. Excessive alkalinity causes irreversible adsorption of CS_2 and intermediate formation (i.e., H_2S and S) in the adsorbent,[16] covering the active sites, which is why the same loading amount of KOH is not as good as K_2CO_3. Consequently, the experimental K_2CO_3 immersion concentration is determined as 0.3 $g\ mL^{-1}$. These results indicate that OH^- on the adsorbent plays a vital role in the adsorption activity.

The C_5 component contains round 80 $\mu g\ mL^{-1}$ of water, so we used the 0.3 $g\ mL^{-1}$ K_2CO_3/Al_2O_3 catalyst to investigate the influence of water. In Fig. 3, as the concentration of added water

Fig. 1 Removal performance of CS_2 over Al_2O_3 modified by different precursors.
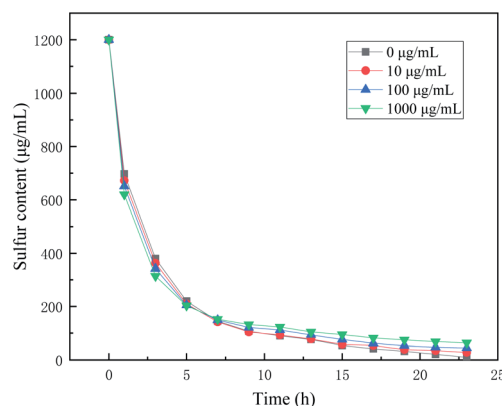
Fig. 3 Effect of water on the removal performance.

increases, the initial desulfurization rate gradually increases, which shows that the addition of water promotes the hydrolysis rate of CS_2. However, with the further progress of desulfurization, CS_2 the final desulfurization result decreases with added water. The water may compete with CS_2 for adsorption, resulting in the weakening of the adsorption capacity of CS_2.[17] The increase in water is also beneficial to the oxidation rate. Primavera *et al.*[18] believed that water plays an essential role in the oxidation of H_2S. The increase of water content can promote the deposition of sulfur products on the catalyst, resulting in an increasing deactivation rate. As the addition of water increases, the water cannot dissolve thoroughly in the C_5, resulting in the separation of oil and water. Therefore, the addition of water cannot improve the performance of the catalyst but reduce the quality of the products.

2.2 Performance of catalysts in fixed-bed reactor

In order to investigate the effect of reaction conditions on the adsorption performance of modified Al_2O_3, the fixed bed was used to study the dynamic adsorption performance of 0.3 g mL^{-1} K_2CO_3/Al_2O_3 catalyst. Fig. 4 shows the effect of (a) sulfur contents, (b) LSHVs, and (c) reaction temperature on the adsorption desulfurization performance in the dynamic desulfurization process of C_5 distillate.

Sulfur content is one of the most important factors affecting the desulfurization capacity of the adsorbent. When the raw material sulfur content is 50, 75, and 100 $\mu g\ mL^{-1}$, the breakthrough sulfur capacity is 0.76 wt%, 0.60 wt%, and 0.46 wt%, respectively. The increase in the sulfur content of C_5 means that H_2S generation increases, which also causes an increase in oxidation products of S and sulfate. The corresponding sulfur products deposit on the surface of the adsorbent, cover the active sites, and hinder the conversion of CS_2. Therefore, the increase of sulfur content in C_5 leads to the decrease of the adsorption desulfurization performance of the adsorbent.

The prepared K_2CO_3/Al_2O_3 adsorbent is used to investigate the effect of different LHSVs on the desulfurization performance of the adsorbents at room temperature. Fig. 4(b) shows that the adsorption capacity of the adsorbent for CS_2 gradually decreases as the space velocity increases. When the space velocity is 0.5, 1.0, and 1.5 h^{-1}, the breakthrough sulfur content is 0.86 wt%, 0.76 wt%, and 0.50 wt%, respectively. When the feedstock feed amount is low, the CS_2 molecule in the C_5 oil has a longer residence time on the surface of the adsorbent, which can promote its adsorption and diffusion process. So, the adsorption performance is better at low space velocity. However, when the space velocity is 0.5 h^{-1}, the amount of raw material oil processed per unit time is too small to meet industrial demand. When the space velocity is too high, the contact time between CS_2 and the surface of the adsorbent is shortened, which is not conducive to the adsorption desulfurization process of the adsorbent. Therefore, it is most suitable for industrial applications when the space velocity is 1.0 h^{-1}.

The prepared 0.3 g mL^{-1} K_2CO_3/Al_2O_3 adsorbent is applied to examine the effect of different adsorption temperatures on the desulfurization performance of the adsorbent at an
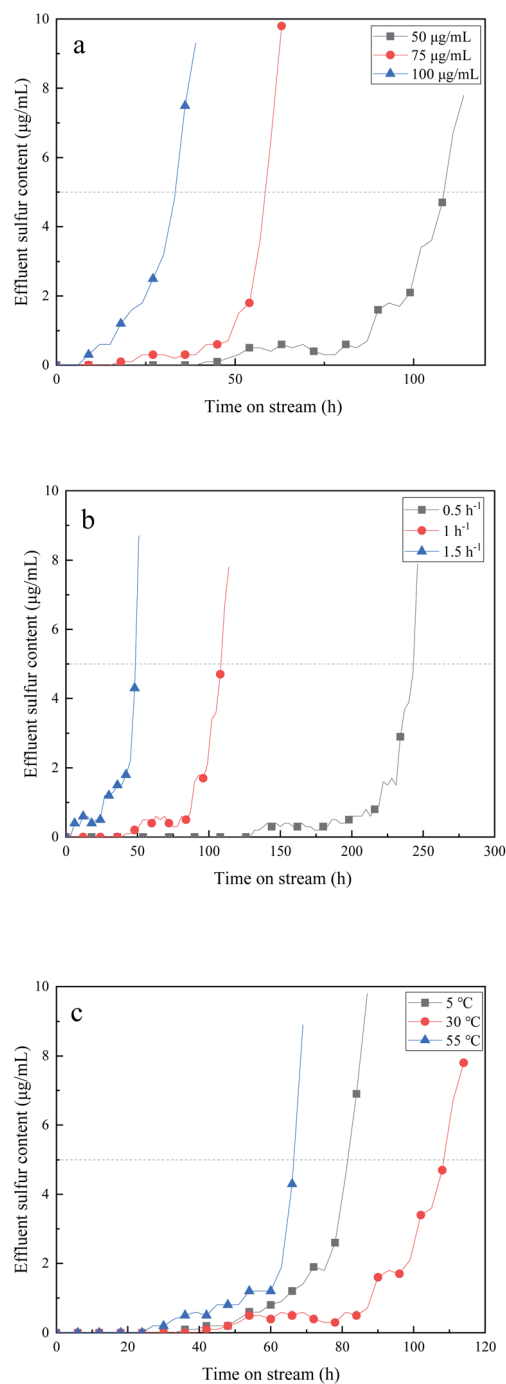

Fig. 4 Effect of (a) sulfur content of raw materials, (b) LHSV, and (c) temperature on removal performance of CS_2.

adsorption LSHV of 1.0 h^{-1}. The influence of temperature on the desulfurization effect is shown in Fig. 4(c). This experiment selects a temperature range of 5–55 °C. At 5 °C, the breakthrough sulfur capacity is 0.57 wt%. It is because the hydrolysis reaction rate of CS_2 in C_5 is low at a relatively lower temperature, resulting in poor desulfurization activity of the adsorbent. With the increase of temperature, the hydrolysis rate increases, and the reaction is more likely to occur. Besides, high temperature also favors the oxidation of H_2S, facilitating the next reaction.

When the temperature is 30 °C, the breakthrough sulfur capacity is 0.76 wt%, and the desulfurization effect is best. The increase in the temperature leads to a gradual rise of SO_4^{2-}/S ratio.[19] Sulfate is formed more rapidly, causing catalyst poisoning and inhibiting the progress of the hydrolysis reaction. When the temperature is 55 °C, the breakthrough sulfur capacity of the adsorbent is 0.47 wt%, which is not suitable for the desulfurization of C_5. Besides, the product begins to turn yellow at 55 °C, indicating that the product has been aggregated, thus affecting desulfurization activity and product quality.

2.3 Evaluation of regeneration performance of adsorbents

The performance evaluation of regenerated adsorbents is carried out in a fixed bed reactor, and its results are shown in Table 1. The evaluation conditions are 30 °C, with a sulfur content of 50 µg mL^{-1} in the raw oil, and an LHSV of 1 h^{-1}. The sulfur capacity of the adsorbent is 0.74 wt% for the first regeneration and 0.71 wt% for the second regeneration. The adsorbent shows good regeneration performance.

2.4 Characterization of the adsorbents

Table 2 shows the pore structure parameters of the adsorbents prepared *via* different concentrations of K_2CO_3. It can be seen from Table 2 that as the K_2CO_3 loading increases, the average pore size increases slightly, while the specific surface area and total pore volume decrease significantly. After loading K_2CO_3, the average pore size increase is due to the pores being filled with K_2CO_3, rather than the pore size becoming larger due to impregnation. The decrease in specific surface area and total pore volume is due to the filling of K_2CO_3, the small pore size disappears, and the large pore size becomes small. When the loading of K_2CO_3 increases from 0.3 g mL^{-1} to 0.4 g mL^{-1}, a large amount of K_2CO_3 is deposited on the surface, the specific surface area decreased from 211.79 m^2 g^{-1} to 158.54 m^2 g^{-1}, and the total pore volume decreased from 0.37 cm^3 g^{-1} to 0.31 cm^3 g^{-1}.

Fig. 5(a) is an isotherm adsorption–desorption curve of different concentrations of K_2CO_3/Al_2O_3 adsorbent. In Fig. 5, the isothermal adsorption–desorption curves of different K_2CO_3/Al_2O_3 adsorbents are type IV and have the same H

Table 1 Breakthrough sulfur capacity of adsorbents with different regeneration times

Regeneration times	0	1	2
Sulfur capacity (wt%)	0.76	0.74	0.71

Table 2 Structural characteristics of prepared K_2CO_3/Al_2O_3 adsorbents

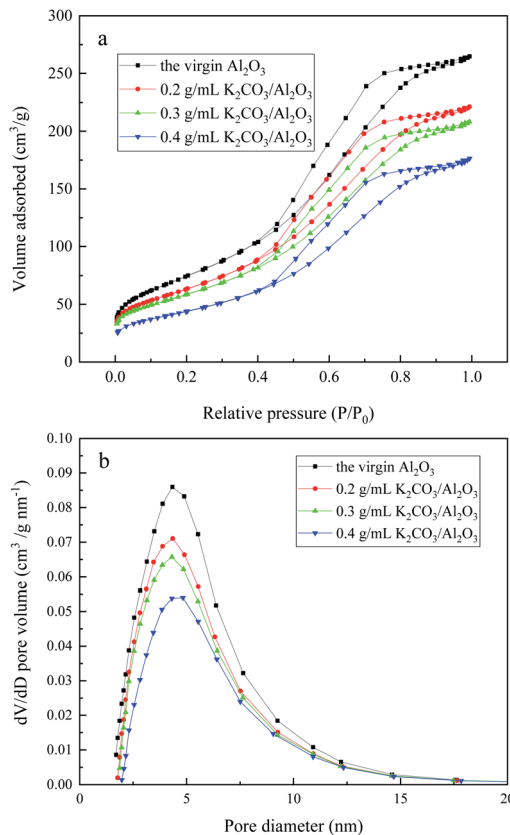| K_2CO_3 concentration (g mL^{-1})	0.0	0.2	0.3	0.4
BET surface area (m^2 g^{-1})	272.09	229.27	211.79	158.54
Total pore volume (cm^3 g^{-1})	0.47	0.39	0.37	0.31
Average pore diameter (nm)	6.02	6.07	6.08	6.89

Fig. 5 (a) Adsorption isotherm and (b) PSD of gamma-Al_2O_3 and supported K_2CO_3 based adsorbents.

hysteresis loop in medium pressure and high-pressure parts ($0.4 < P/P_0 < 1$), which is generally considered to be interconnected by the pore size of the mesoporous material.[20] In the low-pressure section, the adsorption amount is gently increased, and N_2 molecules are adsorbed on the mesopores inner surface in a single layer to a plurality of layers. There is a sudden increase in the adsorption amount at $P/P_0 = 0.4$–0.8, which means that the mesoporous structure is relatively uniform. The pore size distribution of the adsorbent is obtained by the Barrett–Joyner–Halenda method (BJH), which is shown in Fig. 5(b). Interaction between the K_2CO_3 with the support Al_2O_3 does not significantly change the structure.[21] The pore size distribution of the adsorbent loaded with different concentrations of K_2CO_3 is similar, mainly concentrated at 4–5 nm. When the K_2CO_3 loading is 0.3 g mL^{-1}, the pore diameter is the smallest, which is mainly about 4.3 nm. The pore size of this range is suitable for the adsorption of CS_2, and the adsorption desulfurization performance is best.

Fig. 6 shows the SEM image of virgin Al_2O_3, fresh 0.2 g mL^{-1}, 0.3 g mL^{-1}, 0.4 g mL^{-1} K_2CO_3/Al_2O_3 adsorbent and deactivated 0.3 g mL^{-1} K_2CO_3/Al_2O_3 adsorbent. When K_2CO_3 is not loaded, the surface of Al_2O_3 is very rough with a large number of holes, which is an irregular block structure. After the loading of K_2CO_3, the pores of Al_2O_3 are filled with K_2CO_3, and the surface becomes smooth gradually. The unfilled K_2CO_3 is loaded on the surface of the support in the form of small particles. As the

Fig. 6 SEM of (a) the virgin-Al_2O_3, (b–d) the fresh 0.2 g mL^{-1}, 0.3 g mL^{-1}, 0.4 g mL^{-1} K_2CO_3/Al_2O_3, (e) the exhausted 0.3 g mL^{-1} K_2CO_3/Al_2O_3.
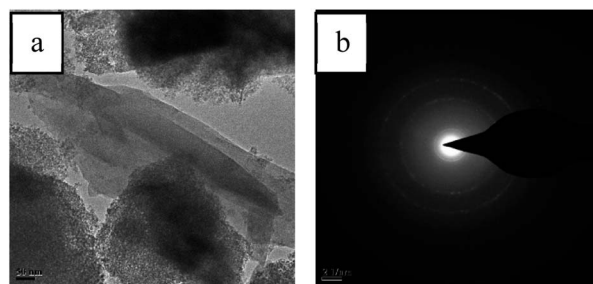

Fig. 7 (a) TEM images of exhausted 0.3 g mL^{-1} K_2CO_3/Al_2O_3 adsorbent and (b) diffraction pattern taken from region c marked in (a).

load increases. When the load concentration of K_2CO_3 is increased from 0.3 g mL^{-1} to 0.4 g mL^{-1}, the mass increase of K is small, probably because the pores are already filled with K_2CO_3, and excessive K species blocks the pores and enriches the surface, resulting in a decrease in the loading mass. When CS_2 is adsorbed, the presence of the S element can be detected, and the mass is 1.23 wt%, which means that the S element can be well adsorbed on the K_2CO_3/Al_2O_3 adsorbent.

Since a newly formed crystal are found in the SEM image after desulfurization, TEM analysis is used. Fig. 7 shows a TEM image of the 0.3 g mL^{-1} K_2CO_3/Al_2O_3 adsorbent adsorbed by CS_2 and a diffraction pattern of the adsorbed product. After the adsorption of CS_2, a wafer appears around the adsorbent, and three crystal rings appear in the diffraction pattern, which is analyzed and calculated. Comparing the calculated Di with the PDF card, it is found that the three Di are 5.756, 1.988, and 1.374, respectively, corresponding to the three diffractive crystal surface (113), (408), and (288) of the S element, which conforms to the S elemental crystal (JCPDS No. 83-2283), demonstrating the formation of elemental S in the products.

Fig. 8 is the CO_2-TPD spectra of the 0.3 g mL^{-1} KNO_3/Al_2O_3, K_2CO_3/Al_2O_3, and KOH/Al_2O_3 adsorbents. For both K_2CO_3/Al_2O_3 and KOH/Al_2O_3 adsorbents, there are two CO_2 desorption peaks at a lower temperature ($\sim$100 °C) and higher temperature ($\sim$600 °C), which belong to the weak base and strong base centers, respectively. Besides, both peak strength and temperature of

loading increased, filamentous K_2CO_3 crystals appeared on the surface of the 0.4 g mL^{-1} K_2CO_3/Al_2O_3 adsorbent.

When 0.3 g mL^{-1} K_2CO_3/Al_2O_3 adsorbent adsorbs CS_2, the product produced by the adsorption process will block the pores and accumulate on the surface, one of the reasons for the decreased activity after adsorption of CS_2.[22] Among them, many kinds of filamentous or banded crystals appear on the surface of the adsorbed Al_2O_3 support. Since the loading of K did not increase, the crystals that appeared are associated with the adsorbed products, and the specific results are further analyzed by TEM.

Table 3 shows the EDS characterization result corresponding to the SEM. Virgin-Al_2O_3 contains only Al and O elements, and other elements are almost zero. After loading K_2CO_3, the content of the K element gradually increases as the amount of

Table 3 EDS analysis of the surface of fresh and exhausted K_2CO_3/Al_2O_3

		Al	O	K	S
Virgin Al_2O_3	at.%	39.62	60.28	0.10	0.01
	wt%	47.33	52.47	0.19	0.01
Fresh 0.2 g mL^{-1} K_2CO_3/Al_2O_3	at.%	36.18	60.25	3.52	0.05
	wt%	46.95	46.35	6.62	0.07
Fresh 0.3 g mL^{-1} K_2CO_3/Al_2O_3	at.%	29.68	62.54	7.74	0.03
	wt%	38.04	47.52	14.38	0.05
Fresh 0.4 g mL^{-1} K_2CO_3/Al_2O_3	at.%	30.47	60.24	9.28	0.01
	wt%	38.25	44.85	16.89	0.01
Exhausted 0.3 g mL^{-1} K_2CO_3/Al_2O_3	at.%	32.34	61.25	5.61	0.80
	wt%	41.60	46.72	10.46	1.23

Fig. 8 CO_2-TPD spectra of 0.3 g mL^{-1} KNO_3/Al_2O_3, K_2CO_3/Al_2O_3, and KOH/Al_2O_3 adsorbents.

KOH adsorbent are higher than those of K_2CO_3, indicating that the alkalinity of KOH/Al_2O_3 is stronger than that of K_2CO_3/Al_2O_3 adsorbent. KNO_3/Al_2O_3 adsorbent has only one weak base and one medium strong base adsorption center, and the desulfurization effect is only improved a little compared with pure Al_2O_3 adsorbent. In the desulfurization process, the hydrolysis center is OH^-, and water plays a role in supplementing OH^-.[23,24] However, high alkalinity is not favorable for the hydrolysis of CS_2 because CS_2 and its final hydrolyzed products (H_2S and CO_2) are easily irreversibly adsorbed on the surface,[16] inhibiting the catalytic hydrolysis reaction. Therefore, the adsorption and hydrolysis capacity of KOH with strong alkalinity is weaker than that of K_2CO_3.

Fig. 9 is an XRD spectrum of K_2CO_3, Al_2O_3 support, fresh 0.3 g mL^{-1} K_2CO_3/Al_2O_3 adsorbent, and exhausted 0.3 g mL^{-1} K_2CO_3/Al_2O_3 adsorbent. The main peaks of pure K_2CO_3 XRD images are at $2\theta = 26.3, 30.1, 32.2, 34.3$, and $42.9°$, which are consistent with PDF cards (JCPDS No. 71-1466).[25] The peaks of the XRD images of the support are mainly at $2\theta = 19.5, 37.6, 39.4, 45.8, 60.8$, and $67.0°$, which is consistent with the position of the main peak of gamma-Al_2O_3 (JCPDS No. 10-0425). Compared with gamma-Al_2O_3, the strength of the main peak after K_2CO_3 modification is lower, and a new K_2CO_3 peak is generated at $2\theta = 32.2$ and $34.3°$. The peak intensity is lower than pure K_2CO_3, which means that K_2CO_3 has a good load on the Al_2O_3 and has good dispersion.[25] Liu et al.[26] found that the K_2CO_3/Al_2O_3 adsorbent after calcining at 500 °C contained K_2O, which may be overlaid in the XRD spectra due to lower content. Therefore, the composition of K_2CO_3/Al_2O_3 adsorbent is K_2CO_3, Al_2O_3, and a small amount of K_2O.

When the adsorbent adsorbs CS_2, no peak of elemental S was found because the generated elemental S is easily sublimated in the air, resulting in too little amount on the surface of the adsorbent being difficult to detect. At $2\theta = 26.4$ and $29.8°$, there is a new peak generation, and the peak intensity at $2\theta = 30.8°$ increases, which is the characteristic peak of K_2SO_4 (JCPDS No. 73-1674), which means the production of SO_4^{2-} after adsorption of CS_2. The peak intensity of Al_2O_3 and K_2CO_3 after adsorption is reduced due to the deposition of sulfur products formed by adsorption of CS_2 on the adsorbents.
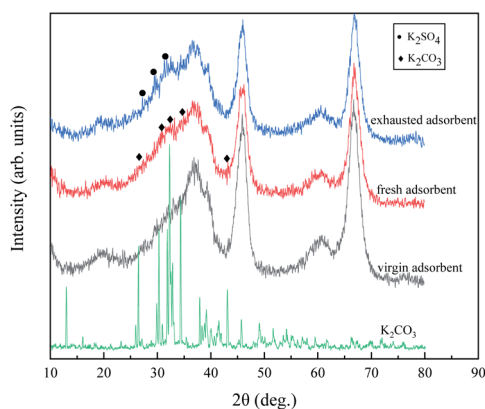
Fig. 10 is a Fourier infrared spectrum of the 0.3 g mL^{-1} K_2CO_3/Al_2O_3 adsorbent before and after the adsorption of CS_2. It can be seen from Fig. 10 that the peak appearing around 3558 cm^{-1} is a characteristic peak of –OH,[27–29] which is derived from the –OH in K_2CO_3/Al_2O_3 adsorbent during catalyst preparation. The peaks at 1400 cm^{-1} and 1580 cm^{-1} are characteristic peaks of –COO and –C=O, which are related to the supported potassium carbonate CO_2.[26] –COO and –C=O promote the oxidation of H_2S, which accelerates the reaction rate of H_2S by O_2 to S, further improving the conversion ability of CS_2. The peaks at 787 cm^{-1} (AlO_4) and 582 cm^{-1} (AlO_6) are related to the Al–O–Al structure.[30]

After adsorption of CS_2, new peaks at 2329 cm^{-1} and 2370 cm^{-1} are related to CO_2,[31] indicating that the CO_2 produced by hydrolysis is chemically adsorbed to the adsorbent. The peaks at 2919 cm^{-1} and 2850 cm^{-1} are related to –CH_3 and –CH_2, indicating the residual of the adsorbed C_5 on the adsorbent. The peaks at 1383 cm^{-1} and 1129 cm^{-1} are related to SO_4^{2-}, which means that sulfite or sulfate may form. The peak at 617 cm^{-1} represents the formation of elemental S,[32] and the adsorbed CS_2 produces elemental sulfur on the surface of the K_2CO_3/Al_2CO_3 adsorbent. This result is consistent with that reported in the literature.[33]

Although we have used XRD and FT-IR to find sulfate group, due to its small content, the peak is not obvious, and it is not
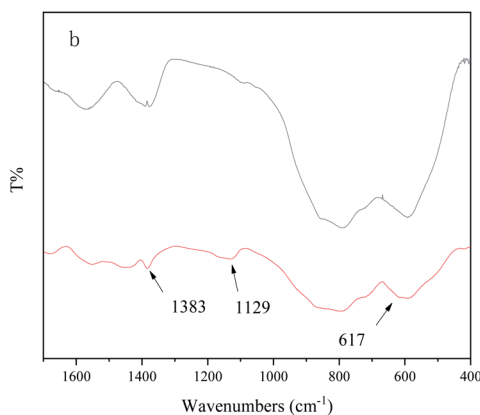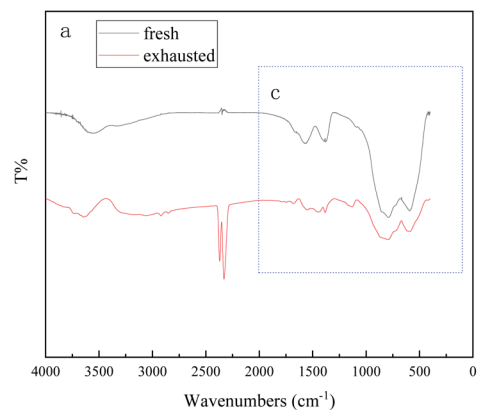

Fig. 9 XRD spectra of the K_2CO_3, the virgin adsorbent, the fresh adsorbent, and the exhausted adsorbent.

Fig. 10 FT-IR spectra of (a) the fresh and exhausted K_2CO_3/Al_2O_3 adsorbents and (b) the enlarged area c marked in (a).

**Table 4** Sulfate and sulfite contents of the fresh and the spent catalysts

	The fresh adsorbent	The spent adsorbent
SO_4^{2-} (wt%)	0.00	2.62
SO_3^{2-} (wt%)	0.00	0.00

possible to distinguish sulfate group from sulfite group. So, the contents of sulfate and sulfite in the fresh and the spent catalysts are analyzed by IC to better explore the sulfur species on the adsorbent. The IC results in Table 4 show that there are no sulfates and sulfites in the fresh adsorbents. The exhausted adsorbent contains 2.62 wt% sulfate but no sulfite. The accumulation of sulfate on the catalyst is the main reason for the decrease of CS_2 adsorption performance.

2.5 Discussion on the reaction mechanism

When the K_2CO_3/Al_2O_3 adsorbent adsorbs CS_2 in C_5, the adsorbent gradually turns yellow due to the accumulation of sulfur on the adsorbent.[34] After adsorbed K_2CO_3/Al_2O_3 is taken out, and it is a yellow granule after grinding. The sulfur smell is dissipated, and the yellow color gradually becomes lighter as time lapses. The adsorbent is further ground to powder. The powder completely turned white after 2 hours, as shown in Fig. 11. This is because CS_2 adsorbs on the adsorbent and is converted into elemental S, and elemental S is disappeared when exposed to the air.

The removal process of CS_2 in C_5 distillate includes three processes of adsorption, hydrolysis, and oxidation. The adsorption is related to the pore structure of Al_2O_3 and active components. The OH^- on the support is mainly derived from K_2CO_3 which is essential for the CS_2 conversion.[35,36] During the hydrolysis process, trace water in the C_5 distillate oil and a large number of OH^- on the adsorbent can hydrolyze CS_2 to H_2S. The
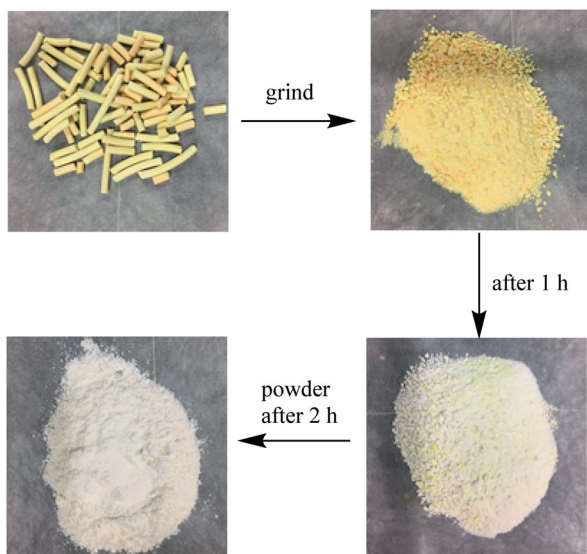
C_5 contains approximately 50–70 µg mL^{-1} of dissolved O_2; the O_2 then oxidizes H_2S to elemental S or SO_4^{2-}, covering the active site of the adsorbent, resulting in a decrease in adsorption capacity.[37] During this period, OH^-, $-COO$ and $C=O$ act to promote oxidation.[38] The specific process is shown in Fig. 12.

3 Methods

3.1 Materials

The pseudo-boehmite powder and sesbania powder were purchased from Shandong Zibo Hengyi Chemical Technology Co., Ltd. K_2CO_3 was purchased from Tianjin Reagent Factory no. 3 Factory (A. R.), and potassium nitrate was purchased from Beijing Chemical Plant (A. R.).

3.2 Preparation of adsorbent

A certain amount of pseudo-boehmite powder was mixed with an appropriate amount of sesbania powder. 2 wt% dilute nitric acid solution was added to the mixed powder and mixed well. After kneading in a squeezer for 90 min, the template was extruded and dried at 120 °C for 12 h followed by calcination in air at 500 °C for 4 hours to prepare strip-shaped gamma-Al_2O_3 support.

The same concentration (0.3 g mL^{-1}) of KNO_3, KOH, K_2CO_3 solution and different concentrations (0.1 g mL^{-1}, 0.2 g mL^{-1}, 0.3 g mL^{-1}, and 0.4 g mL^{-1}) of K_2CO_3 solution were prepared. The gamma-Al_2O_3 support was impregnated with these solutions, respectively, by an incipient-wetness impregnation method, dried at 120 °C for 12 hours, and then calcined at 500 °C for 4 hours to obtain the corresponding potassium salt modified gamma-Al_2O_3 desulfurization adsorbents. They were denoted as 0.3 g mL^{-1} KNO_3/Al_2O_3, 0.3 g mL^{-1} KOH/Al_2O_3, 0.1 g mL^{-1} K_2CO_3/Al_2O_3, 0.2 g mL^{-1} K_2CO_3/Al_2O_3, 0.3 g mL^{-1} K_2CO_3/Al_2O_3, and 0.4 g mL^{-1} K_2CO_3/Al_2O_3. Before the experiments, the catalyst was calcined at 400 °C to remove the H_2O and CO_2.

The regeneration performance of adsorbents was also investigated. The deactivated adsorbents were calcined at 500 °C in the air atmosphere for 3 hours and then cleaned with deionized water for 3 times to remove the deposited sulfate.

Fig. 11 The macro morphology of exhausted adsorbent.
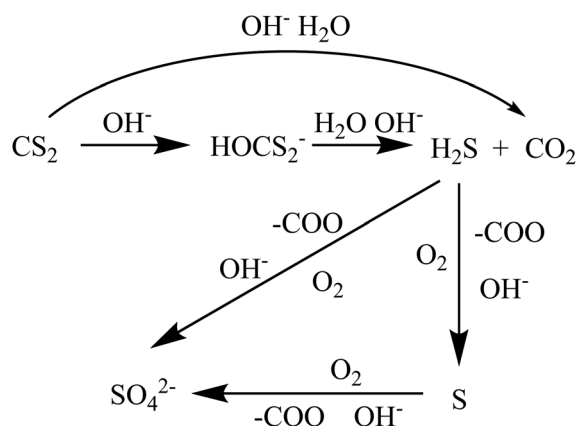
Fig. 12 The mechanism of removal of CS_2 by K_2CO_3/Al_2O_3.

After that, 0.1 g mL^{-1} K$_2$CO$_3$ solution was used for reimpregnation to obtain the regenerated adsorbent.

3.3 Desulfurization performance tests

The cracked C$_5$ distillate was used as raw material, and 0.12 g and 0.005 g of CS$_2$ was added to 100 mL of cracked C$_5$ distillate, respectively. The mixture was stirred until CS$_2$ was completely dissolved. The sulfur contents in the as-prepared C$_5$ oil were 1200 μg mL^{-1} and 50 μg mL^{-1}, respectively. 0.001 g, 0.01 g, and 0.1 g of water were added to 100 mL of prepared C$_5$ distillate, respectively. The final water content of the C$_5$ oil is 10 μg mL^{-1}, 100 μg mL^{-1}, and 1000 μg mL^{-1}, respectively.

The static adsorption method was applied to investigate the adsorption performance of CS$_2$. The experimental conditions were as follows: the adsorption temperature was 30 °C, and 5 g of the modified desulfurization adsorbent was added to 50 mL of C$_5$. The adsorption performance is determined by evaluating the sulfur content of the C$_5$ distillate after adsorption.

The dynamic desulfurization experiment was carried out in a fixed bed reactor at a pressure of 0.4 MPa. The volume of the reaction tube was 30 mL. The sulfur-containing C$_5$ distillate oil is passed through a micro-injection pump from the bottom to the top through a fixed bed with 21 g of modified adsorbent. The effects of temperatures (5, 30 and, 55 °C), different sulfur contents of raw material (50, 75, and 100 μg mL^{-1}), and different liquid hourly space velocities (LHSV) (0.5, 1.0, and 1.5 h^{-1}) on desulfurization performance of the adsorbent were investigated. During the experiment, C$_5$ was collected at the fixed bed outlet at intervals, and the sulfur content was analyzed. When the sulfur content of the C$_5$ was higher than 5 μg mL^{-1}, it was considered that the adsorbent was exhausted, and the experiment was stopped. The calculation formula of the adsorbent breakthrough sulfur capacity S_C (wt%) is shown in eqn (1),

$$S_C = \frac{V(S_{in} - S_{out}) \times t \times 10^{-6}}{m} \times 100 \qquad (1)$$

where V is the inlet flow rate (mL h^{-1}) of C$_5$ distillate, S_{in} and S_{out} are the sulfur content (μg mL^{-1}) of C$_5$ at the inlet and outlet of the reaction tube, respectively. And t is the breakthrough time (h), and m is the mass of the adsorbent (g).

Total sulfur content in the liquid of C$_5$ before and after the reaction was analyzed using an RPP-2000S UV fluorescence sulfur analyzer.

3.4 Characterization of catalysts

The Brunauer–Emmett–Teller (BET) surface area and total pore volume of the adsorbent were measured using an N$_2$ adsorption–desorption apparatus (TriStar II 3020). The total pore volume was calculated by the amount of N$_2$ adsorbed at a relative pressure $(P/P_0) = 0.99$. The total area was calculated using a multipoint BET surface area calculation method. The morphology of the surface of the adsorbent particles was observed by a field emission scanning electron microscope (SEM, Zeiss Sigma 500). The surface elemental analysis of the adsorbents was measured by an energy spectrometer (EDS,

Bruker XFlash 6/30). Transmission electron microscopy image (TEM) was measured using F-20 microscopy (FEI, USA). CO$_2$-TPD was characterized using a Micro Chemics Instrument's Auto Chem II Model 2920 Multi-Function Adsorber. The catalyst was first purged in helium at a temperature of 400 °C for 1 h, cooled to room temperature, and saturated with pure CO$_2$ at a flow rate of 50 mL min^{-1} for 30 min. After that, the TPD experiment was started, the heating rate was 10 °C min^{-1}, the helium flow rate was 50 mL min^{-1}, and the temperature was raised to 800 °C. XRD was characterized by a Panaco Sharp Xpert Pro MPD instrument for fresh K$_2$CO$_3$/Al$_2$O$_3$ adsorbents and exhausted adsorbents. The test conditions were: Cu Kα ray, voltage 36 kV, current 30 mA, scanning range 10–80°, step size 0.02° s^{-1}. The FT-IR was tested using a Nicoleti S50 infrared spectrometer from PerkinElmer. The sample was mixed and milled with KBr before testing, and the infrared wavelength ranged from 4000 to 400 cm^{-1}. Ionic chromatography (IC) was tested by Thermo Dionex ICS-1100. Samples were prepared using 0.10 N NaOH to extract sulfate and sulfite from the spent catalysts using sonication.

4 Conclusions

In this paper, we prepared K$_2$CO$_3$/Al$_2$O$_3$ adsorbents to remove CS$_2$ from C$_5$ distillate. When the K$_2$CO$_3$ loading concentration is 0.3 g mL^{-1}, the desulfurization capacity is the best, and the C$_5$ fraction oil with a sulfur content of 1200 μg mL^{-1} can be desulfurized to below 10 μg mL^{-1}. The use of the adsorbent in a fixed bed reactor also exhibits good adsorptive desulfurization capabilities. When the sulfur content is 50 μg mL^{-1}, the space velocity is 1 h^{-1}, and the temperature is 30 °C, the sulfur content can be reduced to 5 μg mL^{-1} or less and maintained for 108 hours. Under the optimized operating conditions, the breakthrough sulfur capacity is 0.76 wt%. The second and third regeneration capacities of the adsorbent were 74 wt% and 71 wt%, respectively. Based on the evidence of surface chemical characterization data, the removal mechanism of CS$_2$ is proposed. The process of desulfurization of C$_5$ distillate oil includes adsorption, hydrolysis, and oxidation. The adsorption is related to the pore structure of the adsorbents and the active components. The hydrolysis and oxidation processes are consistent with the removal of CS$_2$ in the Claus plant. Further work would be to explore the regeneration mechanism of the deactivated adsorbent.

Author contributions

Xiance Zhang: methodology, investigation, formal analysis, data curation, writing-original draft, Guanglin Zhou: conceptualization, writing-review & editing, project administration, resources, supervision, Mengying Wang: formal analysis, writing-review & editing, Xiaosheng Wang: writing-review & editing, resources, Weili Jiang: writing-review & editing, Hongjun Zhou: supervision.

Conflicts of interest

There are no conflicts to declare.

Acknowledgements

References

1 J. Y. Hou, F. Guo, Q. Hu, Y. Li and Z. M. Hou, *Chin. J. Polym. Sci.*, 2019, **37**, 674–680.

2 H. C. Hsu, S. J. Wang, J. D. Y. Ou and D. S. H. Wong, *Ind. Eng. Chem. Res.*, 2015, **54**, 9798–9804.

3 H. Miki, *J. Jpn. Pet. Inst.*, 2019, **62**, 245–254.

4 D. Salari, A. Niaei, J. Towfighi and P. Panahi, *Iran. J. Chem. Chem. Eng.*, 2006, **2**, 40–51.

5 S. Brunet, D. Mey, G. Pérot, C. Bouchy and F. Diehl, *Appl. Catal., A*, 2005, **278**, 143–172.

6 W. Jiang, X. Gao, L. Dong, J. Xiao, L. H. Zhu, G. Y. Chen, S. H. Xun, C. Peng, W. S. Zhu and H. M. Li, *Pet. Sci.*, 2020, **17**, 1422–1431.

7 Y. Liu, Y. Pan, H. Wang, Y. Liu and C. Liu, *Chin. J. Catal.*, 2018, **39**, 1543–1551.

8 M. A. Larrubia, A. d. Gutièrrez-Alejandre, J. Ramìrez and G. Busca, *Appl. Catal., A*, 2002, **224**, 167–178.

9 C. Li, Z. Jiang, Y. Zhang, Y. Yang, M. Yang and L. Wang, *Chinese Pat.*, CN101450303A, 2009.

10 H. Yu, J. Nan, J. Zhang, Y. Zhang, X. Qu, S. Geng and Y. Shi, *Chinese Pat.*, CN103182291A, 2013.

11 K. Karan and L. A. Behie, *Ind. Eng. Chem. Res.*, 2004, **43**, 3304–3313.

12 C. Deng, X. P. Wu, X. M. Sun, Y. Ren and Y. H. Sheng, *J. Comput. Chem.*, 2009, **30**, 285–294.

13 P. D. Clark, N. I. Dowling and M. Huang, *Appl. Catal., B*, 2001, **31**, 107–112.

14 F. I. Khalili, M. Sultan, C. Robl and M. A. Al-Ghouti, *J. Ind. Eng. Chem.*, 2015, **28**, 282–293.

15 M. Song, X. Yang and G. Wang, *RSC Adv.*, 2018, **8**, 35014–35022.

16 H. Yi, D. He, X. Tang, H. Wang, S. Zhao and K. Li, *Fuel*, 2012, **97**, 337–343.

17 N. Pechler and G. Emig, *Gas Sep. Purif.*, 1991, **5**, 247–251.

18 A. Primavera, A. Trovarelli, P. Andreussi and G. Dolcetti, *Appl. Catal., A*, 1998, **173**, 185–192.

19 L. Wang, D. Wu, S. Wang and Q. Yuan, *J. Environ. Sci.*, 2008, **20**, 436–440.

20 S. Naumov, R. Valiullin and J. Kärger, *Diffus. Fundam.*, 2007, **6**, 67.61–67.62.

21 A. E. Aksoylu, A. N. Akin, S. G. Sunol and Z. İ. Önsan, *Turk. J. Chem.*, 1996, **20**, 88–94.

22 X. Song, K. Li, C. Wang, X. Sun, P. Ning and L. Tang, *Chem. Eng. J.*, 2017, **330**, 727–735.

23 Q. Li, H. Yi, X. Tang, S. Zhao, B. Zhao, D. Liu and F. Gao, *Chem. Eng. J.*, 2016, **284**, 103–111.

24 J. West, B. P. Williams, N. Young, C. Rhodes and G. J. Hutchings, *Catal. Lett.*, 2001, **74**, 111–114.

25 S. C. Lee, Y. M. Kwon, H. J. Chae, S. Y. Jung, J. B. Lee, C. K. Ryu, C. K. Yi and J. C. Kim, *Fuel*, 2013, **104**, 882–885.

26 H. Liu, L. Su, F. Liu, C. Li and U. U. Solomon, *Appl. Catal., B*, 2011, **106**, 550–558.

27 C. Murugan, H. C. Bajaj and R. V. Jasra, *Catal. Lett.*, 2010, **137**, 224–231.

28 S. U. Rege and R. T. Yang, *Chem. Eng. Sci.*, 2001, **56**, 3781–3796.

29 L. Fernández-Carrasco and E. Vázquez, *Fuel*, 2009, **88**, 1533–1538.

30 A. Boumaza, L. Favaro, J. Lédion, G. Sattonnay, J. B. Brubach, P. Berthet, A. M. Huntz, P. Roy and R. Tétot, *J. Solid State Chem.*, 2009, **182**, 1171–1176.

31 K. Li, G. Liu, T. Y. Gao, F. Lu, L. Tang, S. Liu and P. Ning, *Appl. Catal., A*, 2016, **527**, 171–181.

32 M. Liang, C. Li and H. Guo, *J. Fuel Chem. Technol.*, 2002, **30**, 347–352.

33 E. He, G. Huang, H. Fan, C. Yang, H. Wang, Z. Tian, L. Wang and Y. Zhao, *Fuel*, 2019, **246**, 277–284.

34 G. Zhou, Y. Fu and H. Zhou, *Petrochemical Technol.*, 2001, **30**, 602–604.

35 R. Sui, C. B. Lavery, D. Li, C. E. Deering, N. Chou, N. I. Dowling and R. A. Marriott, *Appl. Catal., B*, 2019, **241**, 217–226.

36 Y. Yue, X. Zhao, W. Hua and Z. Gao, *Appl. Catal., B*, 2003, **46**, 561–572.

37 H. Yi, S. Zhao, X. Tang, C. Song, F. Gao, z. Wang, B. Zhang and Y. Zuo, *Catal. Commun.*, 2014, **56**, 106–109.

38 X. Song, P. Ning, C. Wang, K. Li, L. Tang, X. Sun and H. Ruan, *Chem. Eng. J.*, 2017, **314**, 418–433.